Photophysics and dynamics of the lowest excited singlet state in long substituted polyenes with implications to the very longchain limit

Per Ola Andersson and Tomas Gillbro

Citation: The Journal of Chemical Physics **103**, 2509 (1995); doi: 10.1063/1.469672
View online: http://dx.doi.org/10.1063/1.469672
View Table of Contents: http://scitation.aip.org/content/aip/journal/jcp/103/7?ver=pdfcov
Published by the AIP Publishing

Photophysics and dynamics of the lowest excited singlet state in long substituted polyenes with implications to the very long-chain limit

Per Ola Andersson and Tomas Gillbro[a)]
Department of Physical Chemistry, University of Umeå, 901 87 Umeå, Sweden

(Received 28 December 1994; accepted 9 May 1995)

In this paper we explore the intramolecular relaxation processes within two long carotenoids, namely decapreno-β-carotene (M15) and dodecapreno-β-carotene (M19) with 15 and 19 conjugated double bonds (N), respectively. Amplified 200 fs pulses at 590 nm were used to excite the optically allowed $S_0 \rightarrow S_2$ ($1\,^1A_g \rightarrow 1\,^1B_u$) transition of the two carotenoids. The excited state dynamics were probed by continuum light between 400–890 nm in solvents with different polarizabilities. The transient absorption spectra consist of a bleaching region, due to loss of ground state absorption, and of an excited state absorption region at longer wavelengths, due to the $S_1 \rightarrow S_n$ transition. The S_n state was assigned to an $n\,^1B_u$ state. The overall wavelength dependence of the measured kinetics could be well described by introducing three decay time constants. One reflects the S_1 lifetime (τ_1) and was determined to 1.1 and 0.5 ps for M15 and M19, respectively. A second lifetime, between 5 and 15 ps, was attributed to vibrational cooling in the ground state. A third decay time was in the subpicosecond range, and was ascribed to the vibrational redistribution and relaxation of the S_1 potential surface after being populated by the subpicosecond S_2–S_1 internal conversion. No significant change of the decay constants was observed for M15 embedded in a 77 K matrix. This shows that the relaxation rates are only influenced by intramolecular processes. The S_2 lifetime was shorter than the pulse duration and was estimated to be in the order of 100 fs. The $S_0 \rightarrow S_2$ transition of M15 in the liquid phase exhibits a 0.39 anisotropy at short times, while the $S_1 \rightarrow S_n$ transition has an initial value of only 0.31. This corresponds to an angle of 23° between the transition dipoles. The measured S_1 rate constants were analyzed, together with decay constants of shorter carotenes, in terms of the energy gap law. When going from the shortest ($N=5$) to the longest ($N=19$) polyene, τ_1 decreases about 6000 times, i.e., from 3 ns to 0.5 ps. By using an empirical form of the energy gap law the 0–0 transition of $S_1(2\,^1A_g) \rightarrow S_0$ was estimated to be located at 11 300 and $10\,200 \pm 1\,000$ cm^{-1} for M15 and M19, respectively. By fitting the excitation energies of all carotenes in the series ($3 \leqslant N \leqslant 19$) with a truncated two or three term expansion of a power series in $1/N$ the long-chain limit values were extrapolated to be 11 000 and 3 500 cm^{-1} for the $1\,^1B_u$ and $2\,^1A_g$ state, respectively. The implication of these limit values on the electronic structure of polyacetylene are discussed.

INTRODUCTION

Linear polyenes are frequently utilized by nature. Two important examples are the visual chromophore retinal[1,2] and the light-harvesting carotenoids in photosynthetic organisms,[3–5] which both exhibit crucial photophysical properties for their biological function. Other phenomena such as charge transfer and nonlinear optical responses, especially in large conjugated polymer films (as polyacetylene film), have also been the subject of a lot of recent attention.[6,7] Thus it is of great importance to improve our understanding of the electronic structure and photophysical properties of one-dimensional π-conjugated organic molecules. The lowest excited singlet states in discrete linear polyenes with 3–8 conjugated double bonds (N) have been intensely investigated and are also fairly well understood.[8–10] The obtained molecular information has been used to improve our understanding of the electronic properties of very long polyenes such as polyacetylene and related polymers. To obtain a link between well defined discrete polyenes and large polymers we have by time-resolved optical spectroscopy studied two extra long polyenes with 15 and 19 conjugated double bonds. These are two carotenoids homologous to *all-trans*-β-carotene and they are presently the longest discrete polyenes that have been optically investigated. Furthermore, together with the earlier spectroscopically studied carotenes with N varying between 3 and 11,[11] they provide the most extended homologous series that has ever been examined. Therefore, we have in this paper not solely focused our attention to the photophysics and photodynamics of the long carotenes, but also tried to clarify the dependence of the excitation energies and the ultrafast nonradiative processes of the two lowest excited singlet states on the length of conjugation.

Those carotenoids that (in plants, purple bacterial and algae) are involved in energy transfer in photosynthetic antenna complexes usually have 9 to 13 conjugated double bonds and absorb light in the range 400 to 580 nm, due to the strongly allowed optical transition from the ground state (S_0) to the second excited state (S_2).[2–4] In accordance with polyene terminology the S_0 and S_2 states are labeled $1\,^1A_g$ and $1\,^1B_u$, respectively, and, as in linear polyenes, the lowest excited singlet state (S_1) is of $2\,^1A_g$ symmetry. The transition from the ground to the S_1 state is thus by symmetry dipole forbidden and consequently two photon allowed.[8–10] While

a)Author to whom correspondence should be addressed.

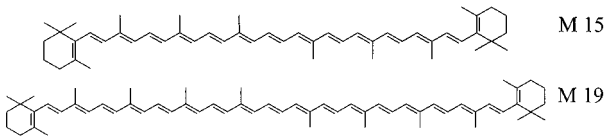

FIG. 1. Molecular structures of the macrocarotenes.

the S_2 state exhibits similar order of single and double bonds as the ground state, the S_1 state has a reversed bond alternation.[9,10]

During the last decades carotenoids have been considered as nonfluorescent, but recently their fluorescence has been observed by several groups.[11–15] The main trend observed in these studies is that carotenoids with $N \geqslant 10$ only show a weak $S_2 \rightarrow S_0$ emission,[12,13] while carotenoids with $7 \leqslant N \leqslant 9$ exhibit a dual emission, (i.e., both S_2 and S_1 emission), and for those with $N \leqslant 7$ the $S_1 \rightarrow S_0$ emission is strongly dominating.[11,14–16] By fluorescence quantum yield measurements the S_2 lifetime of *all-trans-β*-carotene was estimated to be in the order of 100 fs.[11–13,17] A similar value of 200 fs has been obtained from ground state recovery[17] and fluorescent up-conversion[18] experiments. The low $S_2 \rightarrow S_0$ fluorescence yield and the short S_2 lifetime is explained by a strong vibronic coupling to the low-lying S_1 state. The more long-lived S_1 state of *β*-carotene has a lifetime of 8.1 ps at 294 K.[19] It has furthermore been found that the rate of internal conversion between the S_1 and S_0 states increases as N increases, or equivalently as the $S_1 \leftrightarrow S_0$ energy gap decreases,[16,20,21] in accordance to the energy gap law.[22,23] The nonradiative decay rates, however, largely dominate over the radiative rates even for this transition. It is now generally accepted that the accepting mode between S_1 and S_0 is the C═C stretching mode.[19,24–26] In a time-resolved Raman study on *trans-β*-carotene and other naturally occurring carotenoids, evidence has been found that the C═C stretching mode energy is significantly altered, from 1520 to 1780 cm^{-1}, upon $S_0 \rightarrow S_1$ excitation.[24] (The relaxation back to S_0 occurs with a time constant of 10 ps.[24]) This type of shift has also been observed in high resolution fluorescence measurements on the linear polyene, heptaene,[25] and was confirmed by theoretical calculations on a series of polyenes.[26] Furthermore, when *β*-carotene[19] and shorter carotenes,[11,21] homologous to *all-trans-β*-carotene, are embedded in low-temperature matrices, they all show only a weak temperature dependence of the S_1–S_0 nonradiative decay rate, making an involvement of large amplitude motions, as skeletal torsion and bending modes, unlikely.

The fact that the S_1 fluorescence intensity increases as N decreases makes it possible to determine the depopulation rate of S_1 by single photon counting experiments with a time resolution of ca. 10 ps for carotenoids with $N \leqslant 11$.[11] In contrast, the longer carotenoids, decapreno-*β*-carotene ($N=15$) and dodecapreno-*β*-carotene ($N=19$) called M15 and M19, respectively, (where M stands for macrocarotenoid), which are studied in this work (Fig. 1), only show a weak S_2 emission. Therefore, they are better suited for femtosecond ground state recovery (GSR) and $S_1 \rightarrow S_n$ excited state absorption (ESA) experiments. Our time-resolution of about 200 fs is, however, not sufficient to resolve the S_2 lifetimes of M15 and M19. Nevertheless, their low fluorescence quantum yields indicate lifetimes in the order 100 fs.[21] In this work we have therefore concentrated our efforts on the photophysics of the S_1 state and the ground state relaxation for both macrocarotenes. Both solvent and temperature dependence of the relaxation rates have been investigated. The excitation wavelength was normally 590 nm, while the probe wavelength from the continuum light, was varied between 400–890 nm. The overall photophysical process in these carotenes can be summarized as follows: After excitation a S_2 population is created. The vibronic coupling with S_1 depopulates this state via internal conversion with a 100 fs time constant and generates a vibrationally hot S_1 state. This energy is redistributed among vibrational states in S_1 on a subpicosecond time scale and the equilibrated population relaxes on the S_1 potential surface. The S_1 lifetimes of M19 and M15 are 0.5 and 1.1 ps, respectively. The nonradiative coupling totally dominates over the radiative decay and makes the S_1 state nonfluorescent. The S_1 state is depopulated via internal conversion to S_0 and thereby generates a vibrationally hot S_0 state, which thermally relaxes to the ground equilibrated vibrational state within 5–15 ps.

The measured rate of the $2\,^1A_g$–$1\,^1A_g$ internal conversion makes it possible to determine the excitation energy of the $2\,^1A_g$ state with the help of the energy gap law[22,23] as applied on shorter carotenes.[21] The obtained 0–0 energies were 11 300 and 10 200±1 000 cm^{-1} for M15 and M19, respectively. These values were then used together with those of the shorter carotenes for extrapolation to the infinite chain length. The limit energies of $1\,^1B_u$ and $2\,^1A_g$ state were both significantly lower than those found by extrapolating the excitation energy of linear (un)substituted polyenes with N between 3 and 8,[27,28] while the energy difference between $1\,^1B_u$ and $2\,^1A_g$ were roughly equal ($\sim$7500 cm^{-1}). The consequence of these results on the electronic structure of polyacetylene is discussed.

EXPERIMENT

Both compounds used in this study, decapreno-*β*-carotene (M15) and dodecapreno-*β*-carotene (M19), were synthesized by Hoffman–LaRoche Ltd. in Basel, Switzerland. All solvents used were of spectral grade. The sample in a 1 mm cuvette or rotating cell typically had an optical density of 0.3–0.5 at the excitation wavelength. The absorption spectra were always checked before and after the transient measurements. For the 77 K measurements the carotenes were dissolved in 3-methylpentane and placed in a 1 mm glass cell inside an Oxford cryostat.

An amplified femtosecond laser system, generating 200 fs excitation pulses at 580–590 nm and probe light in the range 400–890 nm, allowed us to obtain transient absorption spectra and to measure the kinetics. The 100 ps output pulses at 1064 nm from a cw mode-locked Nd:YAG (model 3800), operating at 82 MHz, were compressed to 3 ps by a fiber-grating compressor. After frequency doubling in a KTP crystal, the light, with average power of 0.9–1.2 W, was synchronously pumping a rhodamine-6G dye laser. The dye laser pulses, usually at 590 nm, were further compressed from 400

to 80 fs. These pulses were then amplified more than 10 000 times by a two-stage dye amplifier (Kiton Red) pumped by a Nd:YAG regenerative amplifier operating at 1 kHz. The amplified pulses of about 20 μJ were divided in two parts by a 50%/50% beam splitter. One beam was used as excitation light and the other beam for generating a white-light continuum, by focusing the pulse into a 1 cm water flow quartz cell. The latter beam was further divided into a probe and a reference beam by a 50%/50% beam splitter. The probe beam was focused to a 0.1 mm spot spatially overlapping with the larger excitation light spot in the sample. The reference beam, however, just passed through the sample cuvette. The probe and reference light beams were collimated and focused onto a grating monochromator with 0.5 mm slits before detection by two different photodiodes. Time delay between the pump and probe pulses was accomplished by a computer controlled optical delay line in the excitation light beam. The pump beam was mechanically chopped. The recorded signal was $\log(I_{pr}/I_{ref})_{EXC.}-\log(I_{pr}/I_{ref})_{NO\ EXC.}$, where I_{pr} and I_{ref} stands for the intensity of the probe and reference pulses, respectively, and the difference of the logarithm of the ratio was calculated for each pair of individually pulses, with and without excitation light. Compensating for the wavelength chirp of the continuum light was done during the measurements of transient absorption spectra. In these experiments the monochromator was computer controlled. The wavelength range and the step size were usually set to 450–850 and 5 nm (or 2 nm), respectively. The pump energy was typically about 3 μJ per pulse. The kinetic data were analyzed and fitted by deconvolution with the measured response function of the system. The response function was measured by probing a high concentrated solution of diphenyl hexatriene in toluene at 500 nm, which gave a two-photon absorption signal.

In the time-resolved anisotropy measurements the polarization of the excitation light was kept either parallel ($I_{\parallel}$) or perpendicular ($I_{\perp}$) to the polarization of the analyzing beam by a Soleilbarbinet compensator. The anisotropy, $r(t)$, was evaluated by the standard expression

$$r(t)=(I_{\parallel}-I_{\perp})/(I_{\parallel}+2I_{\perp}). \quad (1)$$

RESULTS

Absorption spectra

The ground state absorption spectrum of M19 in diethylether, *n*-hexane, toluene and carbondisulfide (Fig. 2) shifts towards longer wavelengths as the solvent polarizability increases, which is well correlated to the refractive index (n) by the term $(n^2-1)/(n^2+2)$. It is a well-known phenomenon for both unsubstituted linear polyenes[8] and carotenoids[29,30] that the dispersive interaction gives rise to this shift for the allowed $1\,^1A_g \rightarrow 1\,^1B_u$ transition. The absorption spectrum of M19 in CS_2 ($n=1.63$) is redshifted with about 1600 cm^{-1} relative to M19 in *n*-hexane ($n=1.37$). Also the so-called uv band, which for M19 is located between 340 and 420 nm, shows a similar dependence on the solvent polarizability, with a corresponding spectral shift between M19 in *n*-hexane and in CS_2 of about 1700 cm^{-1}. Since this transition, which is always observable in absorption spectra of carotenoids, is sensitive to dispersion forces it must be an allowed transition. Therefore, we assigned B_u symmetry to the excited state and the transition of the uv band to $1\,^1A_g \rightarrow 2\,^1B_u$.

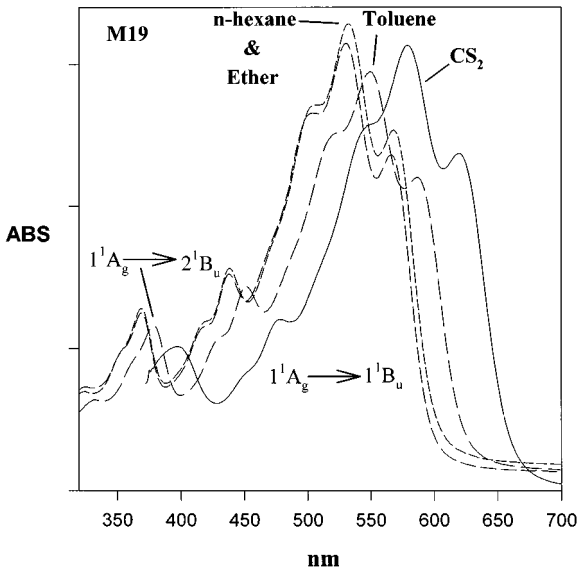

FIG. 2. Absorption spectra of M19 in different solvents.

Spectral shift of transient absorption spectra (TAS)

The transient absorption spectra of M19 dissolved in diethylether, *n*-hexane, toluene and CS_2, respectively, in Fig. 3(a) were measured with a probe pulse delay (Δt) of about 0.4 ps relative to the pump pulse. Similar spectra are shown in Fig. 3(b) for M15 in toluene and CS_2, respectively, again with $\Delta t=0.4$ ps. In the wavelength range of the ground state absorption ΔA $[=A(t)-A(0)]$ is negative, corresponding to a bleaching of the sample, while at longer wavelengths the transient signal is positive, due to excited state absorption (ESA) from the lowest excited singlet state to a higher excited singlet state (S_n). Both the $S_0 \rightarrow S_2$ bleaching and the $S_1 \rightarrow S_n$ transition in the TAS show spectral shifts similar to the ordinary $S_0 \rightarrow S_2$ absorption. These shifts agree with those of β-carotene in *n*-hexane, toluene, and chinoline.[12] The shift between absorption maxima of M19 in *n*-hexane and in CS_2, is about 1500 cm^{-1}, and for M15 in toluene and CS_2, about 900 cm^{-1} (Table I), respectively.

Decay of TAS

In Fig. 4(a) the decay of the transient absorption spectra (TAS) are depicted for M15 in 3-methylpentane glasses and in Fig. 4(b) the formation of the excited state population is shown for M15 in CS_2. The relaxation of the TAS for M19 in toluene and *n*-hexane, is shown in Figs. 5 and 6, respectively. The decay of the TAS was also measured for M15 in toluene and for M19 in CS_2 and diethylether, but these data are not shown. Furthermore, in Fig. 6(b) TAS of M19 measured at relatively long times ($\Delta t \approx 8$–23 ps) are collected. A wavelength dependence of the decay rates is clearly seen for the $S_1 \rightarrow S_n$ transition but not for the $S_0 \rightarrow S_2$ bleaching. The longer the probe wavelength the faster the relaxation of the

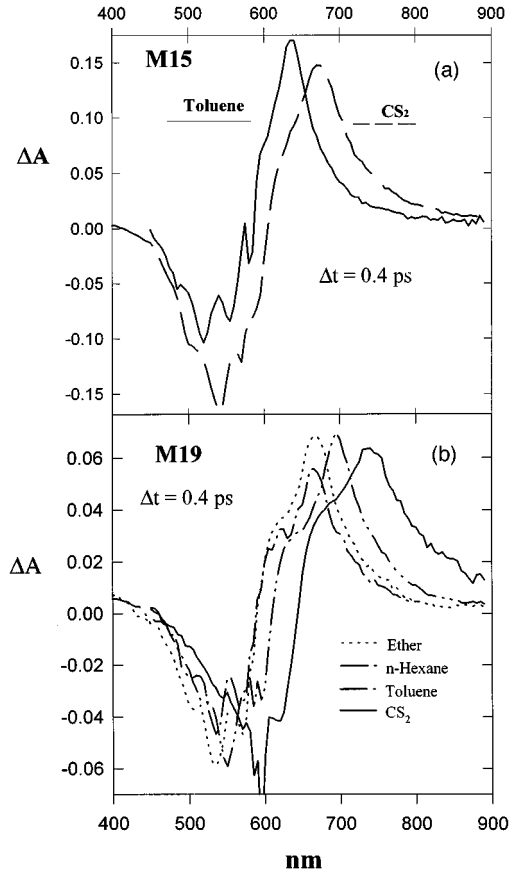

FIG. 3. (a) Transient absorption spectra of M15 in different solvents, measured at $\Delta t \approx 0.4$ ps. (b) Transient absorption spectra of M19 in CS_2 and in toluene, measured at $\Delta t \approx 0.4$ ps.

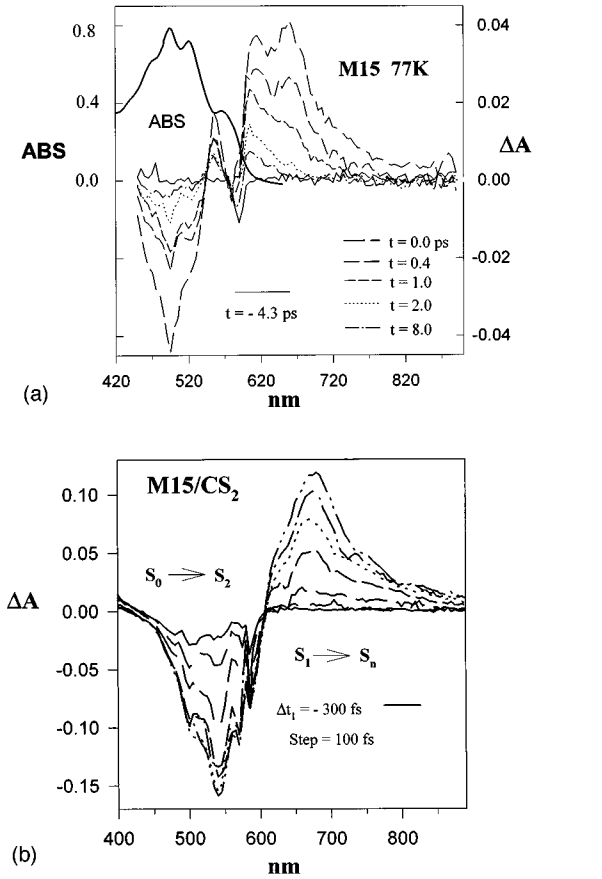

FIG. 4. (a) Decay of transient absorption spectra of M15 in 3-methylpentane glasses at 77 K. (b) Formation of S_2 and S_1 state population of M15 in CS_2 at 295 K.

ESA spectrum. A long-lived component is observed, except at the red part of the ESA [Figs. 4(a), 5, and 6]. All results, irrespective of solvent or temperature, give a very consistent picture of the TAS relaxation. The only anomality is the appearance of an extra band at the red part of the absorption spectrum, close to the excitation wavelength, for M15 in the 77 K glass [Fig. 4(a)], which in turn gives rise to a positive ΔA in the TAS that obviously decays with a longer time constant [Fig. 4(a)].

Kinetics at different probe wavelengths

The kinetics are fitted by one, two, or if necessary three exponentials by deconvolution with the instrument response function (about 200 fs at FWHM), measured at 500 nm (by a two-photon process of a highly concentrated diphenylhexatriene sample). For M15 in toluene the excitation wavelength was about 580 nm, otherwise it was about 590 nm. The calculated time constants are given in Table II. The main conclusion on the feature of the kinetics over the bleaching band is that two decay times are needed for a good fit. One short, about 0.5 and 1.1 ps for M19 and M15, respectively, and one longer component usually about 5–10 ps for both compounds irrespective of the solvent used. The kinetics representing the ESA spectra show a substantial wavelength dependence. At the blue part of the ESA spectrum two and sometimes three time constants are required. Two are similar to those obtained in the bleaching region, i.e., a short 0.5 and 1.1 ps lifetime for M19 and M15, respectively, and one longer component typically about 5–10 ps for both compounds. When a third exponential function is necessary it represents a risetime of $\leqslant$250 fs. As the probe wavelength gets longer the amplitude of the longer component decreases and the short decay time becomes even shorter. In the wavelength region around the absorption maximum of the $S_1 \rightarrow S_n$ transition two decay times are still observed, but further to the red only one short decay time is needed to obtain a good fit. For M19 this time constant is pulse limited ($<$200 fs), resulting in relatively poor fits at short times. Representative kinetic traces are shown in Figs. 7 and 8.

TABLE I. Wavelengths of absorption maxima for different electronic transitions of M19 in different solvents.

	Ether	*n*-Hexane	Toluene	CS_2
$\lambda_{max}(S_0 \rightarrow S_2)$ (nm)	533	530	549	579
$\lambda_{max}(S_0 \rightarrow S_n)$ (nm)	369	369	378	396
$\lambda_{max}(S_1 \rightarrow S_n)$ (nm)	675	675	696	750

Time-resolved anisotropy *r*(*t*)

For M15 in CS_2, $I_{\parallel}$ and $I_{\perp}$ [in Eq. (1)] were measured at several different probe wavelengths, both in the bleaching

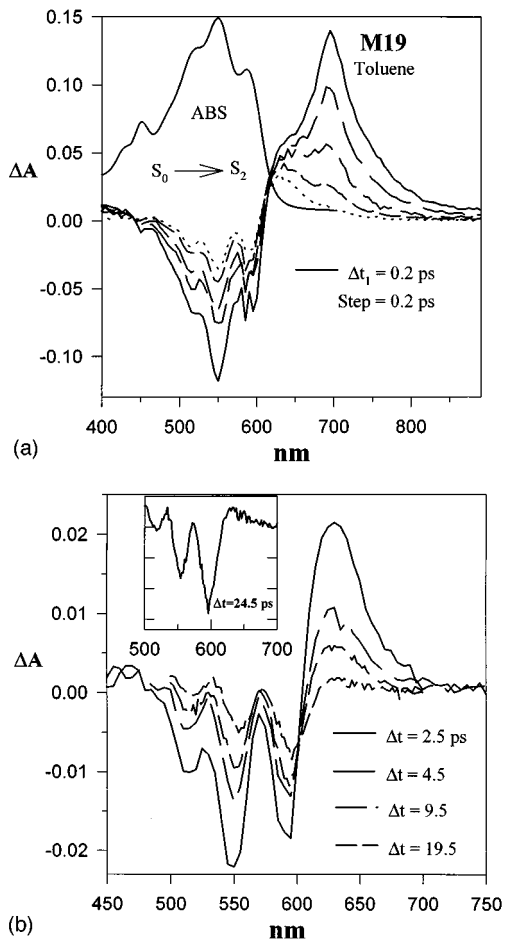

FIG. 5. Decay of transient absorption spectra of M19 in toluene at 295 K. (a) Early times: $0.2 \leqslant \Delta t \leqslant 1.2$ ps. (b) Long times: $2.5 \leqslant \Delta t \leqslant 24.5$ ps.

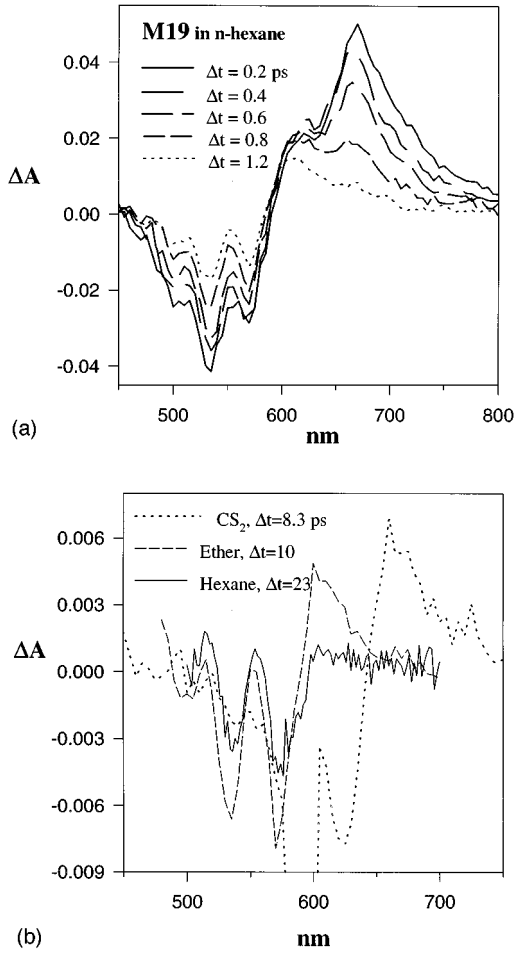

FIG. 6. (a) Relaxation of transient absorption spectra for M19 in *n*-hexane with $0.2 \leqslant \Delta t \leqslant 1.2$ ps. (b) Transient absorption spectra measured at a relatively long Δt for M19 in CS_2, diethylether and *n*-hexane, respectively.

and in the ESA band. Two typical anisotropies with their corresponding isotropic decay ($I_{\parallel}+2I_{\perp}$) are shown in Fig. 8. Over the optical absorption band ($S_0 \rightarrow S_2$) $r(t)$ is constant about 0.39 and for the $S_1 \rightarrow S_n$ transition $r(t)$ initially drops from 0.4 to a constant value of about 0.31. The initial decay occurs within 200 fs, which, as illustrated in Fig. 8(b), corresponds to the rise time of the kinetic of the blue wing decay curve. This rise time represents the S_2 lifetime, but it only sets the upper limit of the real lifetime. The difference in $r(t)$ between the $S_0 \rightarrow S_2$ and $S_1 \rightarrow S_n$ transitions show that these transition dipoles are not parallel. It has been shown that the $S_0 \rightarrow S_2$ transition dipole is parallel to the polyene skeleton[8] and it thus follows that the $S_1 \rightarrow S_n$ transition dipole must deviate somewhat from the polyene backbone in M15.

DISCUSSION

Assignment of the higher excited state in the $S_1 \rightarrow S_n$ transition to a ^1B_u state

The $S_1 \rightarrow S_n$ transition shows the same intensity as the $1\,^1A_g \rightarrow 1\,^1B_u$ absorption in the TAS. This means that the former transition is strongly allowed and possesses a high oscillator strength (about two for the $S_0 \rightarrow S_2$ absorption[29,31]). Since the S_1 state is of A_g symmetry it is likely that the higher excited state (S_n) is of B_u symmetry. Furthermore, the $2\,^1A_g \rightarrow 1\,^1A_g$ emission spectra of shorter carotenes are not sensitive to the solvent induced shift[11,14,21] because of the forbidden character of the transition. This is a well-studied phenomenon for linear polyenes.[8] This means that the higher excited state in the $S_1 \rightarrow S_n$ transition is responsible for the largely solvent polarizability induced shift. This further supports the assignment of S_n as being a B_u state.

The lifetimes of the S_1 and S_2 states and their correlation to ΔE

By high frequency (4 MHz) low-intensity, femtosecond pump–probe measurements at 580 nm we obtained S_1 lifetimes (τ_{f1}) of 470 and 850 fs for M19 and M15, respectively.[32] τ_{f1} of M19 agrees well with the time constants (τ_1) in Table II if the time constants obtained at the red part of the ESA are neglected. The S_1 lifetimes of M15 that we report here are slightly longer, namely about 1.1 ps on average. Also a second longer decay time was observed for both compounds.[32]

In accordance with the energy gap law, which briefly states that the nonradiative rate increases exponentially with decreasing energy gap (ΔE),[22,23] τ_{f1} is shorter for M19 than for M15. This phenomenon has been investigated carefully

TABLE II. Decay times and relative amplitudes of the absorption kinetics at different probe wavelengths for (a) M15 in CS_2 and toluene; (b) M15 in 77 K glasses; (c) M19 in *n*-hexane and ether; (d) M19 in toluene and CS_2. The abbreviation isb stands for isosbestic point.

(a)

λ_{pr} (nm)	M15 in CS_2			M15 in toluene		
CS_2/Tol.	τ_1(ps)/A_1	τ_2(ps)/A_2	τ_3(ps)/A_3	τ_1(ps)/A_1	τ_2(ps)/A_2	τ_3(ps)/A_3
500/500	1.05/−1	10.6/−0.12		1.18/−1	4.2/−0.24	
520/530	1.30/−1	11.8/−0.05		1.10/−1	6.41/−0.22	
540/550	1.29/−1	13.7/−0.15		1.08/−1	8.0/−0.32	
553/−	1.34/−1	18.9/−0.10				
600(isb)/	0.58/−1	6.6/0.62	12.7/−0.39	0.99/−1	7.24/0.20	0.19/−
610						0.84
620/−	1.45/1	12.7/0.23	0.36/−1.32			
640/−	1.37/1	13.9/0.08	0.22/−0.41			
680/680	0.98/1		0.24/−1.14	0.74/1	2.35/0.10	0.16/−0.8
720/750	0.85/1		0.16/−0.95	0.79/1		
800/850	0.82/1					

(b)

	M15 in 3-methylpentane at 77 K					
λ_{pr}(nm)	τ_1(ps)	τ_2(ps)	τ_3(ps)	A_1	A_2	A_3
480	1.08	11.7		−1	−0.29	
500	1.10	8.9		−1	−0.29	
520	0.87	7.4		−1	−0.27	
540(isb)	0.335	1.46		−1	−0.26	
550	3.84	23.2		1	1.86	
560(isb)	0.48	23.8	0.85	−1	0.08	0.51
600	2.05	35.8		1	0.67	
620	1.75	16.0		1	0.34	
680	0.52	2.7		1	0.19	
740	0.52			1		

(c)

λ_{pr} (nm)	M19 in *n*-hexane			M19 in ether		
Hex./Eth.	τ_1(ps)/A_1	τ_2(ps)/A_2	τ_3(ps)/A_3	τ_1(ps)/A_1	τ_2(ps)/A_2	τ_3(ps)/A_3
500/440	0.41/−1	7.0/−0.11		0.42/−1	12.4/0.06	
530/515	0.44/−1	8.5/−0.20		0.58/−1	2.9/−0.18	
566/556	0.61/−1	11.3/−0.21		0.56/−1	1.8/−	
					0.064	
615(isb)/	0.90/1	6.8/0.22		0.41/1	6.54/	0.30/−1.1
605(isb)					0.089	
−/640				0.47/1	6.3/0.051	
670/670	0.24/1			0.30/1		
720/710	0.22/1			0.22/1		
−/750				0.20/1		
800/800	0.20/1			0.17/1		
−/890				0.10/1		

(d)

λ_{pr} (nm)	M19 in toluene			M19 in CS_2		
Tol./CS_2	τ_1(ps)/A_1	τ_2(ps)/A_2	τ_3(ps)/A_3	τ_1(ps)/A_1	τ_2(ps)/A_2	τ_3(ps)/A_3
451/−	0.37/−1					
500/500	0.41/−1	4.0/−	48/0.025	0.60/−1		
		0.094				
522/520	0.49/−1	4.0/−0.11		0.38/−1	2.4/−0.13	
−/540				0.43/−1	4.6/−0.13	
570/575	0.66/−1	3.9/−		0.51/−1	8.7/−0.13	
		0.027				
600(isb)/	0.38/−1	20.0/−		0.58/−1		
600		0.12				
610(isb)/−	2.33/1	45/−0.05				
630/640	0.95/1	6.8/0.23		0.63/−1	1.1/0.68	27.8/−0.3
(isb)						
660/670	0.59/1	7.1/0.056		0.53/1	10.2/0.27	0.33/−1.1
690/700	0.27/1			0.53/1	6.1/0.08	
720/720	0.21/1			0.41/1	7.9/0.017	
750/740	0.21/1			0.38/1		
800/800	0.19/1			0.325/1		
850/850	0.17/1			0.24/1		
890/−	0.12/1					

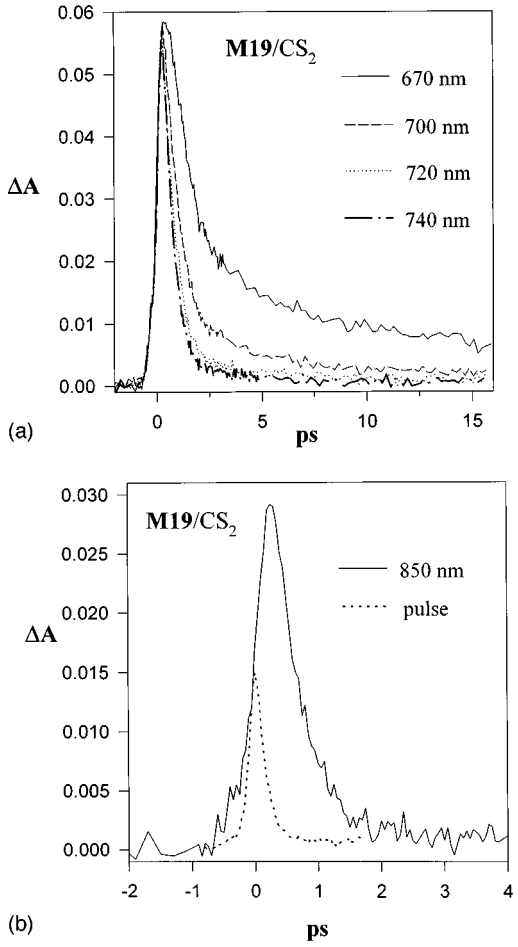

FIG. 7. (a) Kinetics of M19 in CS_2 probed at different wavelengths in the ESA band and in (b) the decay probed at 850 nm is shown together with pulse measured at 500 nm.

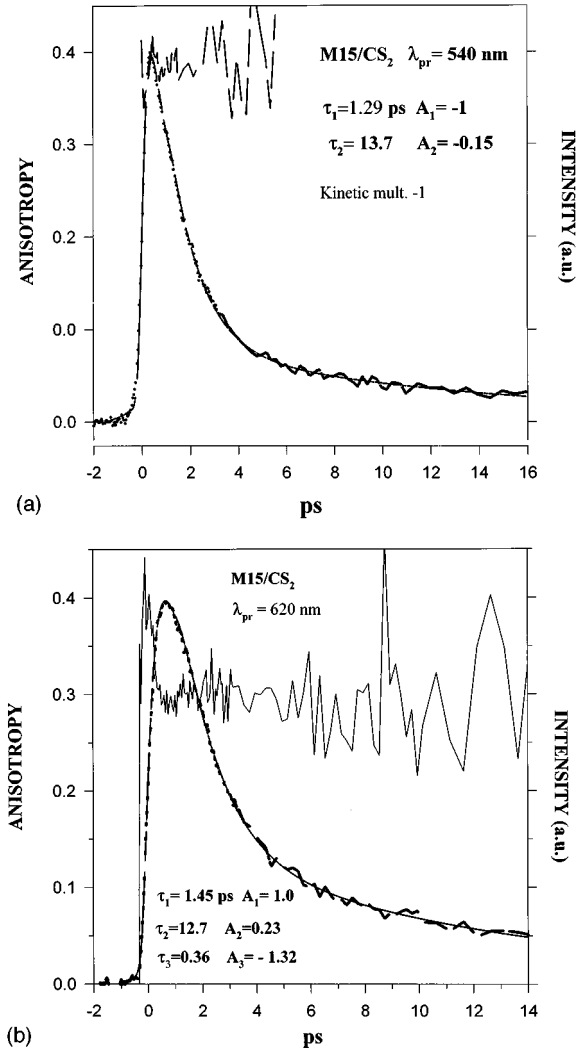

FIG. 8. Isotropic decay with the corresponding anisotropy of M15 in CS_2 probed at (a) 540 nm and at (b) 620 nm.

for a series of carotenes, homologous to *all-trans-β*-carotene, with the number of conjugated double bonds varying between 5 and 11.[21] The rate of internal conversion between S_1 and S_0 (k_1) was determined by the single photon counting technique. The empirical relationship between the logarithm of k_1 and $\Delta E(S_1-S_0)$ is

$$\ln k_1 = 35.9 - 7.39\times10^{-4}\Delta E(S_1-S_0). \tag{2}$$

With $k_1=(0.5\ \text{ps})^{-1}$ and $(1.1\ \text{ps})^{-1}$ this equation predicts a $\Delta E(S_1-S_0)$ of 10 200 and 11 300±1000 cm^{-1} for M19 and M15, respectively. The 0–0 excitation energies of the $1\,^1A_g \rightarrow 1\,^1B_u$ transition measured to 16 700 and 18 000±700 cm^{-1} at 77 K resulting in quite a large energy gap between S_2 and S_1, i.e., about 6800 cm^{-1} for both M19 and M15 in 3-methylpentane glass. Both are larger than the corresponding value $\Delta E(S_2-S_1)\approx5800\ \text{cm}^{-1}$ for *β*-carotene in 77 K glass. The increase in $\Delta E(S_2-S_1)$ with N has, however, been theoretically predicted[8] and experimentally verified for linear polyenes[28] and carotenoids.[14–16]

k_1 decreases about 6000 times when going from the longest ($N=19$) to the shortest ($N=5$) carotene. In agreement with the energy gap law applicated to numerical model calculations on isolated and solvated supermolecules,[23] the variation of k_1 throughout the series should mainly be governed by the energy gap dependence of the Franck–Condon overlap factor. In Fig. 9 are M19 and M15 included in a graph of $\ln k_1$ vs $\Delta E(S_1-S_0)$.

The S_2 lifetimes have been estimated from the fluorescence quantum yields of about 5×10^{-5} for both M19 and M15 to be at least two times shorter than the S_2 lifetime of *β*-carotene, giving $\tau_{f2}\leqslant100$ fs.[21] The fact that k_2 is larger for M19 and M15, despite the fact that their $\Delta E(S_2-S_1)$ is larger than for *β*-carotene, might be due to a competition between internal conversion from S_2 to S_0 with the $S_2\rightarrow S_1$ nonradiative decay channel, due to the relatively small $\Delta E(S_2-S_0)$ in these extra long carotenes.

Relaxation of hot vibrational modes in S_1

The rapidly decaying component at the long wavelength tail in the ESA spectra we ascribe to internal vibrational relaxation in the excited S_1 state. At longer wavelengths a shorter decay time is measured (Table II). In this range the population of vibronically excited S_1 states (S_1^*) are probed, through the $S_1^*\rightarrow S_n$ transition (Fig. 10). Initially the S_2 state is excited and immediately isoenergetical vibrational hot

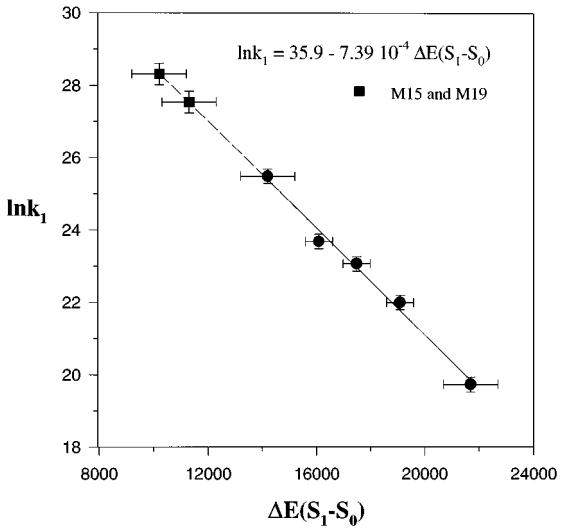

FIG. 9. The natural logarithm of the depopulation rate of S_1 (k_1) vs the energy gap between S_1 and S_0. By extrapolation is the S_1 excitation energy of M15 and M19 determined.

modes in S_1 are populated. This excess energy is redistributed on a subpicosecond timescale and the population relaxes on the S_1 potential surface. At long wavelengths the higher vibrational hot bands are probed and the short decay time detected represents the vibronic relaxation on the S_1 surface. The excess energy is equilibriated and by probing close to the potential well minimum the ultrafast component will vanish. This is clearly the case for M19, especially in a solvent which gives rise to a relatively large $\Delta E(S_2-S_1)$ [Table II(c)]. Any solvent dependence is reflected in the shifts of the $2\,{}^1A_g \rightarrow {}^1B_u$ absorption band and of $\Delta E(S_2-S_1)$.

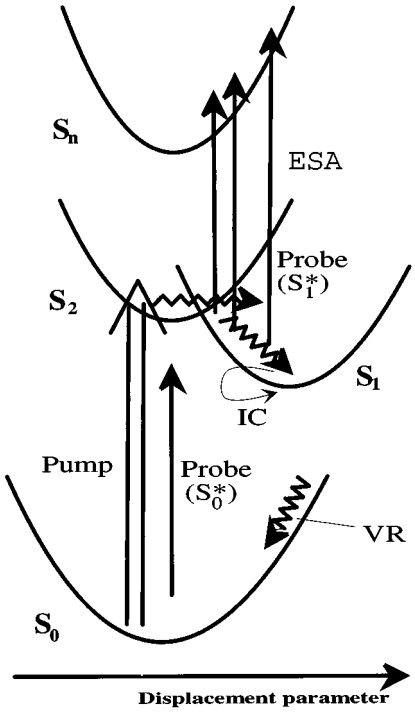

FIG. 10. Schematic picture of potential energy surfaces. Excitation with pump and probe beams, respectively, are represented by straight arrows and the relaxation pathway by other arrows.

Vibrational relaxation in the ground state

We attribute the long time constant in both the GSR and ESA measurements to the vibrational relaxation in S_0. The S_1 level is deactivated by internal conversion to S_0, and the electronic energy of 11 300 and 10 200 cm^{-1} for M15 and M19, respectively, transferred to the vibrational manifold in S_0. The excess energy of the very hot ground state rapidly, on a subpicosecond time scale, equilibrates among neighboring vibronic states, followed by cooling via energy transfer from the solute to the solvent, and finally reaches a thermalized $1\,{}^1A_g$ vibrational population within 5–15 ps. For the GSR decays this process is manifested by the longer bleaching time constant usually about 6–8 ps, while for the ESA decays it results in a similar time constant but with a positive amplitude ($\Delta A>0$). In the latter case the absorption is enhanced due to a population increase of modes that couples to the electronic allowed transition to the S_2 state. This induces a temporary redshift of the absorption spectrum, represented by τ_2 and A_2 (>0) in Table II, which relaxes back to the steady-state absorption spectrum usually within 6–10 ps (Fig. 10).

The overlapping positive and negative signals (ΔA) when probing near the isosbestic (isb) point complicate the analysis. At the red part of the absorption spectrum, where ΔA still is negative, the vibrationally hot absorption gives a positive contribution, which reduces the bleaching signal. On the other hand the ESA signal to the red of the isb will be enhanced by the $S_0^* \rightarrow S_1$ transition. When probing at this position, a rapid decay due to depopulation of S_1 is observed together with a longer time constant associated with $S_0^* \rightarrow S_1$. The amplitude of the longer component is largest close to the absorption spectrum (or isb) and decreases when probing at longer wavelengths, i.e., probing higher vibrational populations on the S_0 potential surface (Fig. 10). No obvious solvent or temperature dependence is observed for the rate of cooling in S_0 (τ_2). For this reason mainly intramolecular relaxation processes are observed. The schematic picture in Fig. 10 summarizes the overall photophysical and dynamical properties of the macrocarotenes as observed in this study.

The obtained ground state vibrational relaxation rate agrees well with the 15 ps decay time of the carotenoid spirilloxanthin, in benzene and toluene, measured by picosecond time-resolved anti-Stokes resonance Raman spectroscopy[33] and also with other large molecules, which usually relaxes thermally within 7–50 ps.[34]

Relaxation rates of M15 in 77 K glasses

For M15 in 77 K glasses the measured time constants are clearly dependent on the probe wavelength. The GSR times are still approximately constant between 480 and 520 nm. The S_1 lifetime τ_1 is about 1.1 ps, which is similar to that obtained for M15 in liquid phase. This is quite unexpected when compared to shorter carotenes. τ_{f1} increases two times for β-carotene[19] and about 2.5–3 times for the

minicarotenes[21] when going from room temperature to 77 K. This indicates that the temperature dependence of τ_1 decreases as N increases. Furthermore, the sensitivity of τ_{f1} to temperature changes shows that the vibrational modes causing the $S_1 \rightarrow S_0$ nonradiative relaxation occur without large structural changes.

No 77 K time-resolved measurements were performed for M19 because of difficulties to dissolve M19 in 3-methylpentane at lower temperatures. Usually aggregates of M19 were formed. It is likely that the same phenomenon occurs for M15, although it was not clearly observed. We believe that the absorption showing up at 570 nm for M15 at 77 K originates from dimers or larger aggregates of M15. This might explain the spectacular transient absorption spectra obtained for M15 in 77 K glasses, shown in Fig. 4(a). Despite a substantial absorption around 550–560 nm the absorption of the sample is enhanced ($\Delta A > 0$) and decays with two time constants, of about 4 and 23 ps, respectively [Table II(b)]. Again, several overlapping signals complicate the analysis. However, one explanation might be that new electronic excited states are generated by aggregation. One state giving rise to the ground state absorption at 550–600 nm and a lower lying more long-lived dark state which could be responsible for the excited state absorption between 550–570 nm. Although the excitation pulses produce scattered light at $\lambda_{exc}=590$ nm it cannot completely explain the distinct fall of ΔA between 555 and 580 nm. The observed band in the TAS is also remarkably narrow, again indicating strong excitonic interaction.[35]

Both τ_1, τ_2, and A_2 continuously decrease over the ESA band between 600 and 890 nm for M15 at 77 K, as illustrated in the TAS of Fig. 4(a) and in Table II(b). Similar explanations as for the liquid phase results for the wavelength dependence of τ_1 and A_2 are also valid here. τ_2 is approximately constant about 9 ps in the GSR decay, while it varies from 36 to 3 ps when going from 600 to 680 nm in the ESA spectrum. We assign the $\tau_2 \approx 9$ ps relaxation time to the cooling of vibrational hot bands in the ground state. The explanation for the extra long τ_2 in ESA we leave open. Perhaps excited states of aggregates with different sizes also exhibit ESA in this wavelength range and decay with different rates.

Time-resolved anisotropy

For M15 in CS_2 we observed a 0.4 anisotropy over the ground state absorption band ($S_0 \rightarrow S_2$) and a lower value, about 0.31, over the ESA band ($S_1 \rightarrow S_n$). With the reasonable assumption that no other depolarizing processes are involved than population transfer between transitions with differently oriented dipole moments in the molecular framework one could calculate the angle (θ) between the intrinsic dipoles of $1\,^1A_g \rightarrow 1\,^1B_u$ and $2\,^1A_g \rightarrow 2\,^1B_u$ transitions by the following expression:[36]

$$r(t) = r = r_0[(3\cos^2\theta - 1)/2]. \tag{3}$$

With $r_0=0.4$ and $r=0.31$, this yields $\theta=23°$. No time-resolved anisotropy measurements were performed for M19, but they have been done for another carotenoid, namely, okenone ($N=11$) in CS_2,[37] with similar results as for M15.

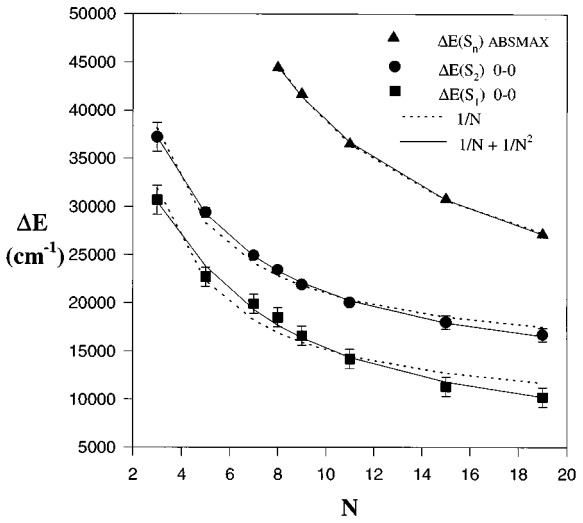

FIG. 11. Measured 0–0 excitation energies for the $2\,^1A_g$ and $1\,^1B_u$ states of the carotenes in 3-methylpentane glasses (except for the $2\,^1A_g$ state of M15 and M19 which were estimated from the energy gap law) are plotted vs the number of conjugation. Also the excitation energies of the $1\,^1A_g \rightarrow 2\,^1B_u$ absorption maximum of the carotenes in room temperature liquids of n-hexane with $N \geqslant 8$ are included. The energies are fitted by a two-term expansion in N^{-1} (---) and by a three-term expansion (—).

Extrapolation of excitation energies to the long-chain limit

The 0–0 excitation energies of the $2\,^1A_g$ and $1\,^1B_u$ states for carotenes in 77 K glasses, and with N varying from 3 to 19, have been collected together with the absorption maximum values of the "uv band" ($1\,^1A_g \rightarrow 2\,^1B_u$) for carotenes with $8 \leqslant N \leqslant 19$ in n-hexane in Fig. 11. Different functions were tested for empirical fitting of the data points: $\Delta E \sim N^{-1}$, $N^{-1}+N^{-2}$, $(N+C)^{-1}$, $N^{-1/2}$, and $(N+C)^{-1/2}$, where C is a fitting parameter. Except for the N^{-1} fit of the S_1 and S_2 energies all functions fit the data points well. However, in accordance to a simple model for linear polyene electronic structure,[27] which briefly is summarized below, we choose N^{-1} or $N^{-1}+N^{-2}$ as fitting functions.

The main goal of the theoretical model was to describe the experimental results of the (0–0) $2\,^1A_g$ and $1\,^1B_u$ excitation energies and then apply it for the long-chain limit.[27] The $1\,^1A_g$ ground state and the $1\,^1B_u$ second excited singlet state were each represented by single configurations: For the $1\,^1A_g$ state all bonding molecular orbitals were doubly occupied and the $1\,^1B_u$ was generated from the ground state configuration by promoting an electron from the HOMO (highest energy occupied molecular orbital) to the LUMO (lowest energy unoccupied molecular orbital). The $2\,^1A_g$ was described as a mixture of the doubly excited (promotion of two electrons from HOMO to the LUMO–Ag2) and the double-jump (promotion of an electron from the HOMO to the LUMO plus one or promotion of an electron from the HOMO minus one to the LUMO–Ag3) configurations. By using Hückel theory and considering electron–electron repulsion which mixes configurations of the same symmetry they computed the energies of these configurations. The mixing was only between the nearly degenerated Ag2 and Ag3 configurations and the corresponding configuration mixing

TABLE III. The excitation energies of $2\ ^1B_u$ (abs. max. in *n*-hexane), $1\ ^1B_u$ (0–0), and $2\ ^1A_g$ (0–0) are fitted by $\Delta E = A + B/N + C/N^2$. The best fit parameters are given together with those obtained by using a two-term expansion, which are shown in the parenthesis.

	$2\ ^1B_u$ (cm^{-1})	$1\ ^1B_u$ (cm^{-1})	$2\ ^1A_g$ (cm^{-1})
A	12 620 (14 570)	10 980 (13 630)	3470 (7790)
B	2.90×10^5 (2.41×10^5)	1.11×10^5 (7.35×10^5)	1.33×10^5 (7.25×10^5)
C	-2.74×10^5	-9.60×10^4	-1.56×10^5

matrix element was empirically set to $\langle \mathrm{Ag2}|\hat{H}|\mathrm{Ag3}\rangle = A + B/N$, where *A* and *B* are two parameters. That the model reproduced all 25 $1\ ^1B_u$ and $2\ ^1A_g$ excitation energies of unsubstituted polyenes, α,ω-diphenylpolyenes and α,ω-dialkylpolyenes with *N* varying between 3 and 8 measured in low-temperature hydrocarbon solutions makes the model reliable. The model was extended for calculations of the $2\ ^1A_g$ and $1\ ^1B_u$ excitation energies in the long-chain limit. For unsubstituted polyenes it resulted in 8710 cm^{-1} and 15 878 cm^{-1} for $2\ ^1A_g$ and $1\ ^1B_u$, respectively. For the α,ω-diphenyl polyenes this calculation was performed by fitting the excitation energies computed for chains with *N* between 3 and 25 to a power series in N^{-1} and then simply letting *N* go to infinity. The limiting values were 8550 and 15 808 cm^{-1} for $2\ ^1A_g$ and $1\ ^1B_u$, respectively.

Accordingly, we fit the carotene excitation energies with a truncated power series in N^{-1}. First with a two-term expansion and then, if necessary, by adding the next term in the power series. The fitted data points are shown in Fig. 11 and the parameters in Table III. All excitation energies were well reproduced by using a three-term expansion in N^{-1}

$$\Delta E = A + B/N + C/N^2. \tag{4}$$

A, *B*, and *C* are treated as parameters in the fitting procedure. The energy difference between $1\ ^1B_u$ and $2\ ^1A_g$ increases as *N* increases and the limiting values (*A*) are 3500 and 11 000 cm^{-1} for the $2\ ^1A_g$ and $1\ ^1B_u$, respectively. These values are significantly lower than those of (un)substituted polyenes. Both $2\ ^1A_g$ and $1\ ^1B_u$ are about 5000 cm^{-1} lower than predicted from discrete polyenes, giving a similar limiting $1\ ^1B_u$–$2\ ^1A_g$ energy gap values for the carotene and polyene series, i.e., about 7500 cm^{-1}. The N^{-1} fitting curves are shown in Fig. 11 and the corresponding parameters, which are given in Table III, agree better with those of finite polyenes. For the $2\ ^1A_g$ and $1\ ^1B_u$ states these two-term expansions only fit the excitation energies relatively well for $N \leqslant 11$, while for $N > 11$ the divergence of the fits from the experimental points increases with increasing *N* (except for the $2\ ^1B_u$ energies which are well reproduced also by two terms in the power series). To really observe this trend it was necessary to introduce the macrocarotenes in the series and thereby extending the upper limit from 11 to 19 conjugated double bonds.

The long-chain limit value of $1\ ^1B_u$ (11 000 $cm^{-1} \approx 1.36$ eV) is very close to the value taken from a room temperature transient absorption spectrum of a polyacetylene film,[38] where the ground state absorption gives rise to a bleaching between 1.1 and 2.1 eV with the minimum located at 1.53 eV. A second band was also observed between 0.2–0.9 eV (1600–7250 cm^{-1}) with a maximum located at 0.48 eV. This induced absorption was later interpreted as excited state absorption from $2\ ^1A_g$ to $1\ ^1B_u$, with the origin of $2\ ^1A_g$ at 1.0 ± 0.1 eV ($\sim$8000 cm^{-1})[39] which was supported by the prediction from the extrapolation of discrete polyene excitation energies.[27,28] This location of $2\ ^1A_g$ in polyacetylene does not fit the long-chain limit value of the carotenes and, besides it does not agree with the fact that the $1\ ^1B_u$–$2\ ^1A_g$ energy gap increases with increasing polyene chain length. It is more likely that the state lies about 7500 cm^{-1} below the $1\ ^1B_u$ state, and thus is almost degenerated with the $1\ ^1A_g$ ground state. If this is true the ESA spectrum of the polyacetylene film must be due to another transition. An explanation might be that another ^1A_g state lies between $1\ ^1B_u$ and $2\ ^1A_g$ in this long polymer, resulting in a $n\ ^1A_g \rightarrow 1\ ^1B_u$ allowed transition that could represent the photoinduced spectrum between 0.2 and 0.9 eV. If so, the origin of this state should be located about 1000–2000 cm^{-1} below the $1\ ^1B_u$ state. In a study of third-harmonic generation in *all-trans*-β-carotene[40] one has interpreted the large nonlinear susceptibility of β-carotene in the visible region as being induced by a strong dipole coupling between the one photon allowed $1\ ^1B_u$ state and a nearby two photon allowed $n\ ^1A_g$ state, which in average was located about 1000 cm^{-1} above the $1\ ^1B_u$ state. Moreover, it has been suggested that this A_g state may approach degeneracy with the $1\ ^1B_u$ state for the long polyenes.[41] Let us assume that the excitation energy of this $n\ ^1A_g$ state decreases faster than the $1\ ^1B_u$ state with increasing *N* in such a way that it changes from lying slightly above $1\ ^1B_u$ in β-carotene to be located about 1000–2000 cm^{-1} below it in polyacetylene, then the $n\ ^1A_g \rightarrow 1\ ^1B_u$ transition could be responsible for the ESA spectrum observed for polyacetylene films.[38] The fact that the $2\ ^1B_u$–$1\ ^1B_u$ energy gap decreases from 16 500 to 10 400 cm^{-1} when going from β-carotene ($N=11$) to M19 clearly shows that the excitation energies of different electronic states exhibit different dependence on the length of conjugation. Therefore, one has to account for the possibility that an electronic state located slightly above $1\ ^1B_u$ in discrete polyenes might be located slightly below $1\ ^1B_u$ state in for example polyacetylene and to fully understand the electronic structure of large polymers it is of great importance to reveal the dependence of excitation energies on the length of conjugation for different excited singlet states.

CONCLUSIONS

By a femtosecond amplified laser system a white light continuum was generated for probing the long carotenes, decapreno-carotene ($N=15$) and dodecapreno-carotene ($N=19$), called M15 and M19, respectively, between 400–890 nm, and thereby follow their relaxation back to the ground state after excitation, with 200 fs pulses at 590 nm, of the allowed $S_0 \rightarrow S_2$ optical to the ground state after excitation, with 200 fs pulses at 590 nm, of the allowed $S_0 \rightarrow S_2$ optical allowed transition. The measured transient absorption spectra show a bleaching region, due to the $S_0 \rightarrow S_2$ absorption, and of an excited state absorption due to the $S_1 \rightarrow S_n$ transition at longer probe wavelengths. The fact that the latter transition is

strongly allowed, and that it shows a similar dependence on solvent polarizability as the former, and that the S_1 state is of $1\,^1A_g$ symmetry, makes it very reasonable to assign S_n to the ^1B_u point group.

Three distinct different decay times were obtained. The first time constants reflects the real lifetime of the lowest lying excited state ($\tau_1=\tau_{f1}$), which was determined to be about 0.5 and 1.1 ps for M19 and M15, respectively.

The second, longer (τ_2) decay time was attributed to the vibrational cooling in the ground state after being populated by internal conversion from S_1. GSR measurements monitored the relaxation back to the lowest vibrational states in $1\,^1A_g$. When probing to the red of the steady-state absorption spectrum a hot vibrational population in S_0 (S_0^*) is promoted to the S_2 state, which contributes to a temporary redshift of the absorption spectrum. The longer the used probe wavelength the hotter is the vibrational population probed in S_0. In the red wing of the ESA spectrum this signal goes to zero.

The third decay time in the subpicosecond range is assigned to the vibrational relaxation in the excited state S_1 (S_1^*), which is observed only in the red part of the ESA spectrum. Vibrationally hot populations are probed and excited to S_n. The observed decay times represent the vibrational redistribution and relaxation on the S_1 potential surface, after being rapidly populated by S_2–S_1 internal conversion.

The S_2 lifetime is probably 100 fs or shorter for both the investigated compounds[21] and the measured time-resolved anisotropy of the $1\,^1A_g\rightarrow 1\,^1B_u$ and the $2\,^1A_g\rightarrow 2\,^1B_u$ transition shows that their intrinsic dipole moments differs about 23°, with the former parallel to the polyene chain.

By using an empirical form of the energy gap law obtained from shorter carotenes with $5\leqslant N\leqslant 11$ the excitation energies of $1\,^1A_g\rightarrow 2\,^1A_g$ transition (0–0) were calculated to 11 300 and $10\,200\pm 1000$ cm^{-1} for M15 and M19, respectively. By successfully fitting the excitation energies of all carotenes in the series ($3\leqslant N\leqslant 19$) with a truncated three term expansion of a power series in $1/N$ the long-chain limit values were extrapolated to be 11 000 and 3500 cm^{-1} for $1\,^1B_u$ and $2\,^1A_g$, respectively. The implication of these limit values on the electronic structure of polyacetylene was discussed.

ACKNOWLEDGMENTS

We are grateful to the Swedish Natural Science Research Council, the Swedish Technical Science Research Council, The Human Science Frontiers Program, and the Kempe Foundation for financial support. We also thank Hoffman–LaRoche for the gift of the macrocarotenes and Eva Åkesson for giving helpful technical know-how.

[1] R. R. Birge, Annu. Rev. Phys. Chem. **41**, 683 (1990).
[2] Y. Koyama and Y. Mukai, in *Advances in Spectroscopy*, Vol. 21, edited by R. J. H. Clark.
[3] R. J. Cogdell and H. A. Frank, Biochim. Biophys. Acta **895**, 63 (1987).
[4] D. Siefermann-Harms, Biochim. Biophys. Acta **811**, 325 (1985).
[5] R. van Grondelle, J. P. Decker, T. Gillbro, and V. Sundström, Biochim. Biophys. Acta **1187**, 1 (1994).
[6] A. J. Heeger, S. Kivelson, J. R. Schrieffer, and W.-P. Su, Rev. Mod. Phys. **60**, 781 (1988).
[7] P. Tavan and K. Schulten, Phys. Rev. B **36**, 4337 (1987).
[8] B. S. Hudson, B. E. Kohler, and K. Schulten, in *Excited States*, Vol. 6, edited by E. C. Lim (Academic, New York, 1982), p. 1.
[9] B. E. Kohler, in *Conjugated Polymers*, edited by J. L. Bredas and R. Silbey (Kluwer Academic, Netherlands, 1991), p. 405.
[10] G. Orlandi, F. Zerbetto, and M. Z. Zgierski, Chem. Rev. **91**, 867 (1991).
[11] P. O. Andersson, T. Gillbro, A. E. Asato, and R. S. H. Liu, J. Lumin. **51**, 11 (1992).
[12] S. L. Bondarev, S. M. Bachilo, S. S. Dvornikov, and Tikhomirov, J. Photochem. Photobiol. **46**, 315 (1989).
[13] T. Gillbro and R. J. Cogdell, Chem. Phys. Lett. **158**, 312 (1989).
[14] S. A. Cosgrove, M. A. Guite, T. B. Burnell, and R. L. Christensen, J. Phys. Chem. **94**, 8118 (1990).
[15] B. DeCoster, R. L. Christensen, R. Gebhard, J. Lugtenburg, R. Farhoosh, and H. A. Frank, Biochim. Biophys. Acta **1102**, 107 (1992).
[16] T. Gillbro, P. O. Andersson, R. S. H. Liu, A. E. Asato, S. Takaishi, and R. J. Cogdell, Photochem. Photobiol. **57**, 44 (1993).
[17] A. P. Shreve, J. K. Trautman, T. G. Owens, and A. C. Albrecht, Chem. Phys. Lett. **178**, 89 (1991).
[18] H. Kandori, H. Sasabe, and M. Mimuro, J. Am. Chem. Soc. **116**, 2671 (1994).
[19] M. R. Wasielewski, D. G. Johnson, E. G. Bradford, and L. D. Kispert, J. Chem. Phys. **91**, 6691 (1989).
[20] H. A. Frank, R. Farhoosh, R. Gebhard, J. Lugtenburg, D. Gosztola, and M. R. Wasielewski, Chem. Phys. Lett. **207**, 88 (1993).
[21] P. O. Andersson, S. M. Bachilo, R.-L. Chen, and T. Gillbro, J. Phys. Chem. (submitted).
[22] R. Englman and J. Jortner, J. Mol. Phys. **18**, 145 (1970).
[23] M. Bixon, J. Jortner, J. Cortes, H. Heitele, and M. E. Michel-Beyerle, J. Phys. Chem. **98**, 7289 (1994).
[24] T. Noguchi, H. Hayashi, M. Tasumi, and G. H. Atkinson, Chem. Phys. Lett. **175**, 163 (1990).
[25] J. H. Simpson, L. McLaughlin, D. S. Smith, and R. L. Christensen, J. Chem. Phys. **87**, 3360 (1987).
[26] F. Negri, G. Orlandi, F. Zerbetto, and M. Z. Zgierski, J. Chem. Phys. **91**, 6215 (1989).
[27] B. E. Kohler, J. Chem. Phys. **93**, 5838 (1990).
[28] B. E. Kohler, C. Spangler, and C. Westerfield, J. Chem. Phys. **89**, 5422 (1988).
[29] P. O. Andersson, T. Gillbro, L. Ferguson, and R. J. Cogdell, Photochem. Photobiol. **54**, 353 (1991).
[30] T. Noguchi, H. Hayashi, M. Tasumi, and G. H. Atkinson, J. Phys. Chem. **95**, 3167 (1991).
[31] J. Applequist, J. Phys. Chem. **95**, 3539 (1991).
[32] T. Gillbro, P. O. Andersson, R. S. H. Liu, A. E. Asato, and R. J. Cogdell, in *Frontiers of Photobiology*, edited by A. Shima, M. Ichahashi, Y. Fujiwara, and H. Takebe (Elsevier, Amsterdam, 1993), p. 25.
[33] H. Hayashi, T. L. Brack, T. Noguchi, M. Tasumi, and G. H. Atkinson, J. Phys. Chem. **95**, 6797 (1991).
[34] T. Elsaesser and W. Kaiser, Annu. Rev. Phys. Chem. **42**, 83 (1991).
[35] *Organic Molecular Aggregates*, Springer Ser. Solid-State Sciences, Vol. 49, edited by P. Reineker, H. Haken, and W. C. Wolf (Springer, Berlin, 1983).
[36] J. R. Lakowicz, *Principles of Fluorescence Spectroscopy* (Plenum, New York, 1983).
[37] P. O. Andersson, T. Gillbro, and R. J. Cogdell (unpublished).
[38] J. S. Horwitz, B. E. Kohler, and T. A. Spiglanin, J. Phys. (Paris) C **7**, 381 (1985).
[39] B. E. Kohler, J. Chem. Phys. **88**, 2788 (1988).
[40] J. B. van Beek, F. Kajzar, and A. C. Albrecht, J. Chem. Phys. **95**, 6400 (1991).
[41] S. N. Dixit, D. Guo, and S. Mazumdar, Phys. Rev. B **43**, 6781 (1991).